arXiv:1702.07378v1 [physics.bio-ph] 22 Feb 2017

Selection of the tagged photons by off axis heterodyne holography in Ultrasound-modulated optical tomography

M. Gross[1]

[1] *Laboratoire Charles Coulomb - UMR 5221 CNRS-UM2 Université Montpellier Place Eugène Bataillon 34095 Montpellier, France*

Ultrasound-modulated optical tomography (UOT) is a technique that images optical contrast deep inside scattering media. Heterodyne holography is a promising tool able to detect the UOT tagged photons with high efficiency. In this work, we describe theoretically the detection of the tagged photon in heterodyne holography based UOT, show how to filter the untagged photon, and discuss the effect of shot noise. The discussion considers also speckle decorrelation. We show that optimal detection sensitivity can be reached, if the frame exposure time of the camera used to perform the holographic detection is of the order of the decorrelation time.

OCIS codes: 170.1650, 170.3660, 290.7050, 090.0090, 170.7050

I. INTRODUCTION

Light scattering prevents optical imaging deep inside scattering media. UOT (ultrasound-modulated optical tomography) [1, 2] also called acousto-optic imaging [3], has been developed to overcome this limit by combining ultrasonic defined spatial resolution and optical contrast (i.e. sensitivity to the bulk optical properties like absorption). One of the purpose of the technique is to use the optical contrast to detect breast tumors that cannot be seen with ultrasound, because the ultrasound contrast is too low. In an UOT experiment, the light scattered through a diffusing sample cross an ultrasonic beam, and, due to the acousto-optic effect, undergoes a frequency shift equal to the ultrasonic frequency [4, 5]. By detecting the frequency-shifted photons, called tagged photons, and by plotting their weight as a function of the ultrasonic beam geometry, 2D (two dimensions) or 3D (three dimensions) images of the sample can then be obtained with an ultrasonic spatial resolution.

Various methods have been developed to detect the very low tagged photon signal out of a large background of untagged photons [2, 3]. First experiments use single pixel detector and detection of the tagged photon AC modulation at the ultrasonic frequency [4, 6, 7]. Since each speckle grain oscillates with a different phase, the single pixel method detects, with a good efficiency, no more than one speckle grain. This severely limits the detection etendue (the etendue is a property of light in an optical system defined as the product of the detection area and the acceptance solid angle: see `https://en.wikipedia.org/wiki/Etendue`). To increase the detection etendue without reducing the modulation depth, three types of methods have been developed. The first type relies on incoherent detection with a narrow spectral filter (∼MHz) that filter out the untagged light. A large area single pixel detector can be used. Examples include Fabry-Perot interferometers [8–10] and spectral hole burning [11–13] based methods. These techniques require bulky and expensive equipment. The second and third types of method use interferences and are thus sensitive to the signal phase decorrelation due to the living tissue inner motions, and to the corresponding Doppler broadening. For breast, this broadening is 1.5 kHz [14]. The second method is based on a photorefractive crystal, which records the volume hologram of the sample scattered field. This hologram can be then used to generate a diffracted field able to interfere with the scattered field on a large area single-pixel detector [15–18]. The method has a large optical etendue ($\sim 10^8$ speckle), but is somewhat sensitive to decorrelation, since the response time of the crystal is usually much longer than the speckle correlation. Promising results are expected with Sn2P2S6:Te and Nd:YVO4 crystals, because of their short response times [19, 20].

The third type of method uses a pixel array, i.e., a camera, to detect the UOT tagged photons [21–24]. The optical etendue ($\sim 10^5$ to 10^6 speckles) is then related to the number of pixels of the camera. The camera method has been improved by adapting the heterodyne holography technique [25] to the tagged photon detection [26]. By tuning the LO (local oscillator) beam frequency near the ultrasonic sideband, and by using a properly adjusted spatial filter, the tagged photons were detected selectively. Moreover, optimal noise detection was obtained, since shot noise is the dominant noise in heterodyne holography [27–29].

In reference [26], the UOT tagged photon detection was nevertheless performed with a gel phantom sample. The acquisition time (~ 1 s) was shorter than the gel decorrelation time (~ 10 s), but much longer than the decorrelation time *in vivo* (< 1 ms). Since [26], it was generally considered [30] that heterodyne holography UOT cannot be used with a sample, whose decorrelation time is shorter than the time needed to record several camera frames. It results that heterodyne UOT has been virtually abandoned. Very recently, several groups [30, 31], have solved this supposed decorrelation problem by performing heterodyne holography UOT with a lock-in camera, which makes the four phase demodulation very fast, within the camera electronics.

In this work, we show that the decorrelation problem

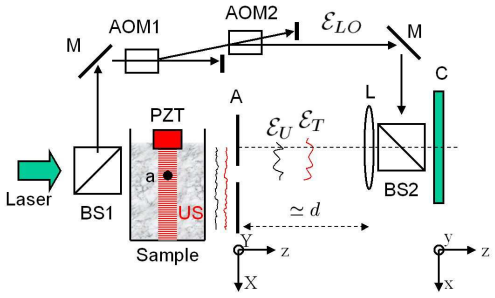


FIG. 1. Typical UOT setup: BS1, BS2: beam splitter; M: mirror; AOM1,AOM2: acousto optic modulator; PZT: piezoelectric transducer that generates the US (ultrasonic) beam; a: absorber embedded in the diffusing sample; A: rectangular aperture; L: lens; C: camera; $\mathcal{E}_{LO}, \mathcal{E}_T, \mathcal{E}_U$: LO, tagged and untagged fields.

does not exist. We show that heterodyne UOT can detect the tagged photon efficiently if the decorrelation time is of the order of the exposure time of a single frame of the camera (which can be order of magnitudes shorter that the acquisition time of several frames). The use of a lock-in camera is thus not essential.

To get this result, we have developed a theoretical framework that describes the ref. [26] detection scheme in detail. We showed how the untagged photons can be efficiently filtered off, and we calculated how the UOT signal is affected by untagged photons, speckle noise, shot noise, etendue and decorrelation .... By comparing results obtained with and without decorrelation, we show that heterodyne holography remains, with decorrelation, an optimal detection scheme of the tagged photons. Note that this point has been already demonstrated for the detection of the untagged photon, in experiments done without ultrasound [32–37].

We finally validate our theoretical analysis by comparing a theoretical simulation with the experimental results of reference [26].

II. THE HETERODYNE HOLOGRAPHY UOT SETUP OF REF.[26]

To introduce our theoretical discussion, let us consider the heterodyne holographic UOT setup of ref. [26] (see Fig. 1). A laser of frequency ω_L is split by the beam splitter BS1 into a signal beam and a local oscillator (LO) beam. The signal beam travels through the diffusing sample S and is scattered by it. The sample is explored by an US (ultrasonic) beam of frequency ω_{US}. The light transmitted by the sample exhibits to components. The first component at $\omega_T = \omega_L + \omega_{US}$ is weak ($\sim 10^{-2}$ to 10^{-4} in power), and corresponds to the tagged photons that have interacted with the US beam. The second component at $\omega_U = \omega_L$ is the main one ($\simeq 100\%$ in power). It corresponds to untagged photons which have not interacted with US.

Heterodyne detection	Filtering in time: $\Delta\varphi \gg 1$
$\omega_{LO} \simeq \omega_T$	tagged photon are selected
$\omega_{LO} \neq \omega_T$	untagged photons are filter off
$\mathcal{E}_{LO}$ large	gain: G=$\lvert\mathcal{E}_T\mathcal{E}_{LO}\rvert/\lvert\mathcal{E}_T\rvert^2 \gg 1$
Holographic image of A	Filtering in space
	$\lvert x_i\rvert > \lvert x_i - x_o\rvert$ and $\lvert x_o\rvert < \lvert w/2\rvert$
A off axis	tagged signal is off-axis
	while untagged signal is on-axis
A narrow	tagged, untagged and LO
	shot noise signals are separated

TABLE I. Detection of the tagged photons.

A rectangular aperture A located off axis near the sample, control the size and location of the zone of the sample where the tagged and untagged fields $\mathcal{E}_U$ and $\mathcal{E}_T$ are detected. A lens L of focal d located at a distance $|\mathrm{AL}| \simeq d$ of A collects the light. The beam splitter BS2 mixes $\mathcal{E}_T$ and $\mathcal{E}_U$ with the LO field $\mathcal{E}_{LO}$ whose frequency ω_{LO} is controlled by AOM1 and AOM2 (acousto optic modulator or bragg cell) . To detect the tagged photons, $\omega_{LO} \simeq \omega_T$.

The camera C ($N \times N$ pixels) records a sequence of M frames I_m (with $m = 0...M-1$) corresponding to the interference pattern: $\mathcal{E}_T + \mathcal{E}_U + \mathcal{E}_{LO}$. Frame I_m is recorded at time $t_m = m\Delta t$, where $\Delta t = 2\pi m/\omega_C$ is the pitch in time, and ω_C the camera frame frequency. The hologram H_C of the aperture A (that is back illuminated by $\mathcal{E}_T$ and $\mathcal{E}_U$), in the camera plane C, is calculated by combining frames I_m. The hologram H_A, in the aperture plane A, is then calculated from H_C. The signal of interest (tagged photon) is calculated from H_A.

III. DETECTION OF THE TAGGED PHOTONS

A. Principle of UOT detection

The UOT detection is illustrated by table I. The goal is to measure the energy of the tagged photons $|\mathcal{E}_T|^2$ which is very low. To detect selectively the tagged photons, UOT perform a double filtering (in time and space), with gain.

The time filtering is made by the camera, which records the tagged, untagged and LO interference pattern. The camera signal is thus $|\mathcal{E}_T + \mathcal{E}_T + \mathcal{E}_{LO}|^2$. It results that $\mathcal{E}_T$ is detected by heterodyne detection. The tagged photons are selected ($\mathcal{E}_T\mathcal{E}_{LO}$ varies slowly since $\omega_{LO} \simeq \omega_T$), while the untagged photons are filtered off, ($\mathcal{E}_U\mathcal{E}_{LO}$ varies fast since ω_{LO} and ω_T are very different). This time filtering is characterized by the phase drift $\Delta\varphi$ of the untagged photons during the measurement time. We have: $\Delta\varphi \simeq M\omega_{US}\Delta t \gg 1$.

Since the local oscillator field $\mathcal{E}_{LO}$ is much larger than the tagged photon field $\mathcal{E}_T$, the heterodyne detection

(whose signal corresponds to $\mathcal{E}_T\mathcal{E}_{\mathcal{LO}}$) is made with heterodyne gain of $G = |\mathcal{E}_T\mathcal{E}_{LO}|/|\mathcal{E}_T|^2 \gg 1$.

The space filtering is made by the aperture A, whose image is reconstructed by digital holography. Indeed, the camera signal is also a hologram of the aperture, which is back illuminated by the tagged field $\mathcal{E}_T$. By reconstructing the holographic image of the aperture, one can separate the tagged, tagged LO noise signals. The tagged photons correspond to the image of the aperture, which is a bright band located off axis, the untagged photons yield a parasitic signal located on axis, while the shot noise is a background which is spread out everywhere : see Fig. 7 (b) [26]. This spatial filtering is characterized by 3 parameters: x_i and x_o and w. x_i and x_o are the inner and outer coordinates of the aperture edges (with respect to the detection optical axis), and $w = N\Delta X$ is the width of the holographic reconstructed image in plane A. Here, ΔX, given by Eq.4, is the size of the reconstructed pixels, and $N \times N$ is the number of pixels. To perform an efficient spatial filtering, the aperture A must be within the holographic reconstructed image: $|x_o| < |w/2|$, and off-axis enough (with respect to its width): $|x_i| > |x_i - x_o|$.

B. Outline of the UOT simulation

Our goal is to analyse the signals that are obtained in the heterodyne UOT experiment of Fig. 1 in order to understand how the the tagged photon signal can be detected selectively. Our analyse is made in several steps.

(a) We assume first that the tagged and untagged speckle fields scattered by the sample in the plane of the aperture A are known. These fields, which are random, are calculated within plane A.

(b) We calculate the tagged and untagged fields in the camera plane C by field propagation from A to C.

(c) We assume then that the LO field, which is flat field, is known. We calculate, for each frame m, the intensity I_m corresponding to the sum of the tagged, and untagged and LO fields on each pixel of the camera, and we convert the optical signal into photo electrons.

(d) We add to the photo electron signal I_m of each frame and each pixel, a random noise corresponding to shot noise, which is the dominant noise in heterodyne holography [27–29]. We get I'_m.

We then model the data analysis made in the UOT experiment of reference [26].

(e) We consider all frames I'_m of the sequence, and we calculate the hologram H_C of the light scattered by the sample.

(f) We propagate H_C from the camera plane C to the aperture plane A yielding the reconstructed hologram H_A.

(g) We select within H_A the tagged photon signal and to calculate its weight.

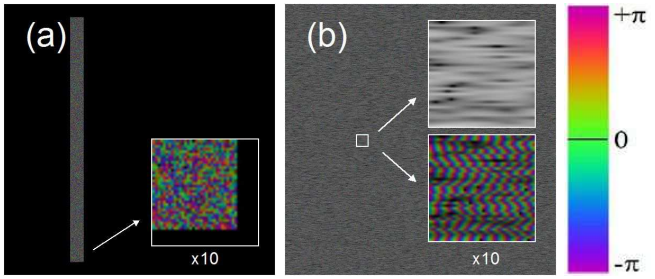


FIG. 2. (a) Image and ×10 zoom (insert) of the tagged or untagged fields in the aperture plane plane A i.e. $E_{A,T}(X, Y, t_m)$ or $E_{A,U}(X, Y, t_m)$. Brightness is amplitude in arbitrary logarithmic scale. Color is phase. The coordinates of the upper left and bottom right corner of the aperture are (250,50) and (300,974). The calculation grid is 1024×1024 pixels. (b) Image and ×10 zoom (insert) of the tagged or untagged fields in the camera plane plane C i.e. $E_{C,T}(x, y, t_m)$ or $E_{C,U}(x, y, t_m)$. The upper zoom is amplitude alone in arbitrary logarithmic scale for intensity.

C. Notations

Let us first define the notations for the LO, untagged and tagged fields in planes A and C. We have:

$$\begin{aligned}
\mathcal{E}_{C,LO}(x, y, t) &= E_{LO}\ e^{j\omega_{LO}t} + \text{c.c.} \qquad (1)\\
\mathcal{E}_{A,U}(X, Y, t) &= E_{A,U}(X, Y, t)\ e^{j\omega_L t} + \text{c.c.}\\
\mathcal{E}_{A,T}(X, Y, t) &= E_{A,T}(X, Y, t)\ e^{j(\omega_L+\omega_{US})t} + \text{c.c.}\\
\mathcal{E}_{C,U}(x, y, t) &= E_{C,U}(x, y, t)\ e^{j\omega_L t} + \text{c.c.}\\
\mathcal{E}_{C,T}(x, y, t) &= E_{C,T}(x, y, t)\ e^{j(\omega_L+\omega_{US})t} + \text{c.c.}
\end{aligned}$$

where c.c. is the complex conjugate. Here, $\mathcal{E}_{...}$ are optical fields (which evolve at the optical frequencies ω_L, $(\omega_L + +\omega_{US})$ or ω_{LO}), while $E_{...}$ are complex amplitudes (which are slow varying with time). X, Y are the coordinates in plane A, and x, y the coordinates in plane C. We have used different notations for plane A and C, because the pitches of the calculation grid are different in plane A and C. To simplify theory, we have considered here that E_{LO} is flat field, and propagates along the z direction. E_{LO} do not depend thus on x, y and t.

D. The fields in plane A without and with decorrelation

In plane A, the tagged and untagged photon fields are fully developed speckle. The complex fields are $E_{A,T}(X, Y, t_m)$ and $E_{A,U}(X, Y, t_m)$ are thus random Gaussian complex quantities that are uncorrelated from one pixel (X, Y) to any other $(X', Y') \neq (X, Y)$. These fields are calculated by Monte Carlo on a discrete calculation grid with $N \times N$ pixels of pitch ΔX. Because of the aperture A, the fields $E_{A,T}(X, Y, t_m)$ and $E_{A,U}(X, Y, t_m)$ are zero out of the aperture.

1. If the experiment is made with a gel sample, whose speckle remains correlated with time, the random amplitudes $E_{A,T}(X,Y,t_m)$ and $E_{A,U}(X,Y,t_m)$ do not depend on the recording time t_m of frame m.

2. On the other hand, if the experiment is made with a living sample, whose scatterers move, we will consider that the speckles are totally decorrelated from one frame to the next. The random fields $E_{A,T}(X,Y,t_m)$ and $E_{A,U}(X,Y,t'_m)$ are then totally uncorrelated if $t_m \neq t_{m'}$.

Figure 2 (a) shows an example of tagged or untagged fields $E_{A,T}(X,Y,t_m)$ or $E_{A,U}(X,Y,t_m)$ calculated by Monte Carlo. As seen in the $\times 10$ zoom, the phase is random from one pixel to the next.

E. The tagged and untagged fields in plane C

In the UOT setup of Fig.1, the lens L, which is located near the camera, and whose focal plane is close to plane A, collects the tagged and untagged fields. Because of lens L, the tagged and untagged fields in planes C and A are related by a Fourier transform

$$\begin{aligned} E_{A,T}(X,Y) &= \tilde{E}_{C,T}(k_x,k_y) = \mathrm{FFT}(E_{C,T}(x,y)) \quad (2)\\ E_{A,U}(X,Y) &= \tilde{E}_{C,U}(k_x,k_y) = \mathrm{FFT}(E_{C,U}(x,y)) \end{aligned}$$

where FFT is the discrete Fourier transform operator. The coordinates (X,Y) in plane A are related to the Fourier space coordinates (k_x,k_y) by:

$$(X,Y) = (k_x,k_y) \times |\mathrm{CA}|/k \quad (3)$$

where $|\mathrm{CA}|$ is the camera to aperture distance and $k = 2\pi/\lambda$.

Figure 2 (b) shows the tagged or untagged fields $|E_{C,T}(x,y,t_m)|^2$ or $|E_{C,U}(x,y,t_m)|^2$ in the camera plane. The image exhibits a speckle that is uniformly distributed on the calculation grid that corresponds to the camera detector area. To better visualize this speckle $\times 10$ zooms are displayed in the square inserts. Since the aperture is vertical, the speckles are elongated in the horizontal direction x (see upper insert), but because of the off axis location of the aperture, the phase varies very fast, and increases along the x direction, within each speckle. Indeed, in the lower insert the colors are displayed in green, red, blue order from left to right.

F. Pixel, etendue, modes and camera low pass filtering

In equation 2, the FFT is calculated within a calculation grid that fits with the camera pixels. The pitch Δx of the discrete coordinates x,y is thus equal to the size of the pixel of the camera. Because of the FFT, the pitch ΔX in plane A is

$$\Delta X = 2\pi|\mathrm{CA}| \ /(Nk\Delta x) \quad (4)$$

where $N \times N$ is the number of pixels of the camera ($N = 1024$ typically). The detection etendue G is thus

$$\begin{aligned} G &= S_A S_D/|\mathrm{CA}|^2 \quad (5)\\ &= N^2\lambda^2 \end{aligned}$$

where $S_A = N^2|\Delta X|^2$ and $S_C = N^2|\Delta y|^2$ are the areas of the calculation grid in plane A and C.

The number of modes or speckle grains that can be detected is equal to the number of pixels of the camera: N^2, i.e. to the number of pixels of the calculation grid in plane A and C. Equation 5 means that the etendue of each pixel of planes A, or C is equal to λ^2, i.e. to the etendue of one mode. We must nevertheless notice that the fields in plane A ($E_{A,T}$ and $E_{A,U}$) vary very fast in the X and Y directions. Indeed, because these fields results from the scattering by a think diffusing sample, their correlation length is about λ. The spatial variations of these fields are thus considerably faster than the pitch ΔX of the measurement grid.

To solve this paradox, we must remark that the camera plays the role of a low pass filter that selects the slow varying components (in space) of the fields in plane A. Indeed, the fields $E_{A,T}$ and $E_{A,U}$ are scattered in all directions, and most of the scattered photons never reach the camera. The photons, which do not reach the camera correspond to the fast varying components of $E_{A,T}$ and $E_{A,U}$. The camera area is a low pass filter that selects the low spatial frequency components of the fields $E_{A,T}$ and $E_{A,U}$, which are sampled by pixels of size $\Delta X \gg \lambda$. The fields $E_{A,T}$ and $E_{A,U}$ that are considered correspond to these slow components.

This analysis is confirmed by the energy conservation in planes A and C, since we have, because of the FFT Percival relation:

$$\sum_{X,Y} |E_{A,U\mathrm{or}T}(X,Y)|^2 = \sum_{x,y} |E_{C,U\mathrm{or}T}(x,y)|^2 \quad (6)$$

G. The camera frame signals I_m

The frame signal I_m corresponds to the sum of the tagged, untagged and LO fields. To detect the tagged photons, ω_{LO} is made close to the tagged photon frequency $\omega_L + \omega_{US}$. The tagged photons field E_T thus interfere with E_{LO}, and E_T and E_{LO} must be summoned in field. On the other hand, the untagged photon field E_U does not interfere with E_{LO} and E_T. E_U can be summoned in intensity. We have thus:

$$\begin{aligned} I_m(x,y) &= |E_{C,T}(x,y,t_m) + c^m E_{LO}|^2 \quad (7)\\ &\quad + |E_{C,U}(x,y,t_m)|^2 \\ &= (c^m E^*_{LO} E_{C,T}(x,y,t_m) + \ \text{c.c.}) \\ &\quad + |E_{LO}|^2 + |E_{C,T}(x,y,t_m)|^2 \\ &\quad + |E_{C,U}(x,y,t_m)|^2 \end{aligned}$$

where c is the LO versus tagged field phase shift that correspond to one time step Δt:

$$c = e^{j(\omega_{LO}-\omega_{US}-\omega_L)\Delta t} \tag{8}$$

In equation 7, the useful terms that are $c^m E^*_{LO} E_{C,T}$ and $c^{-m} E_{LO} E^*_{C,T}$. These terms are enhanced because of the high power of the local oscillator E_{LO} (i.e. the holographic gain $|E^*_{LO} E_{C,T}|/|E_{C,T}|^2$ is much larger than one).

The term $c^m E^*_{LO} E_{C,T}$ is the $+1$ grating order term, which proportional to $E_{C,T}$. This term is displayed on Fig.2(b). Similarly, the term $c^{-m} E_{LO} E^*_{C,T}$ is the -1 grating order term. The terms $|E_{LO}|^2$ and $|E_{C,T}|^2$ are zero grating order terms. $|E_{LO}|^2$ is large, but flat field, while $|E_{C,T}|^2$ is small, and can be neglected. Finally, the term $|E_{C,U}|^2$ is an untagged photon spurious, which is most often much larger than the useful term $c^m E^*_{LO} E_{C,T}$, because $|E_{C,U}|^2 \gg |E_{C,T}|^2$. This spurious must be filtered off.

H. The shot noise

Because of the random nature of light emission and camera photo conversion, the frame optical signal I_m is affected by shot noise yielding the frame detected signal I'_m:

$$I'_m(x,y) = I_m(x,y) + s(x,y,m)\sqrt{I_m(x,y)} \quad) \tag{9}$$

where the term $s\sqrt{I_m}$ accounts for shot noise. Here, I_m must be expressed in photo electron Units per pixel and per frame, while s is a real Gaussian random variable of variance $\langle s^2 \rangle = 1$ uncorrelated with pixels (i.e. X, Y) and with frames (i.e. with m).

I. The holograms in plane A and C and the selection of the tagged photons

The tagged photon signal can be extracted from the measured data by calculating the hologram H_C in the camera plane C, and by propagating H_C from the camera plane C to the aperture plane A yielding H_A. The way this procedure is done depends on the decorrelation of the speckle.

We will show first how H_C and H_A are calculated without and with decorrelation (see section III I 1 and section III I 3). To illustrate how the tagged photons are selected without and with decorrelation, we will consider examples, in which the shot noise is neglected (see section III I 2 and section III I 4).

1. *Calculation of the holograms without decorrelation*

Let us first consider a sample whose speckle remains correlated with time. The holograms in plane C and A are thus $H_{C,\text{corr}}$ and $H_{A,\text{corr}}$. The recorded data are analyzed by four phase detection at the tagged photon frequency. We have

$$\omega_{LO} = \omega_{LO,\text{corr}} = \omega_L + \omega_{US} + \omega_C/4 \tag{10}$$

yielding $c = -j$ in Eq. 7. The hologram $H_{C,\text{corr}}$ is calculated from a sequence of M frames, where M is a multiple of four. We have:

$$H_{C,\text{corr}}(x,y) = \sum_{m=0}^{M} j^m I'_m(x,y) \tag{11}$$

The hologram $H_{A,\text{corr}}$ is calculated from $H_{C,\text{corr}}$ by Fourier transform:

$$\begin{aligned} H_{A,\text{corr}}(X,Y) &= \tilde{H}_{C,\text{corr}}(k_x,k_y) \\ &= \text{FFT}\left(H_{C,\text{corr}}(x,y)\right) \end{aligned} \tag{12}$$

2. *Example of hologram calculated without decorrelation and without shot noise*

To illustrate how the tagged photons can be selected, let us consider that the shot noise can be neglected. Let us assume $I'_m = I_m$.

With this hypothesis, the terms $|E_{LO}|^2$, $|E_{C,U}|^2$ and $|E_{C,T}|^2$ of Eq.7 do not contribute to $H_{C,\text{corr}}$, because they do not vary with time t_m. Moreover, the order -1 term $c^{-m} E_{LO} E^*_{C,T}$ yields zero in the summation of Eq.11, because $j^m c^{-m} = -1^m$. Finally, the $+1$ term contributes alone. We have:

$$\begin{aligned} H_{C,\text{corr}}(x,y) &\simeq M E^*_{LO} E_{C,T}(x,y) \\ &\propto E_{C,T}(x,y) \end{aligned} \tag{13}$$

The hologram $H_{C,\text{corr}}$ is thus proportional to the field $E_{C,T}$, which is displayed on Fig.2. From Eq.2, Eq.13 and Eq.12, we get:

$$\begin{aligned} H_{A,\text{corr}}(X,Y) &\simeq M E^*_{LO} E_{A,T}(X,Y) \\ &\propto E_{A,T}(X,Y) \end{aligned} \tag{14}$$

The reconstructed hologram $H_{A,\text{corr}}$ is thus proportional to the tagged field $E_{A,T}$. The image displayed in in Fig. 2(a) corresponds thus both to $E_{A,T}$ and to $H_{A,\text{corr}}$.

3. *Calculation of the holograms without decorrelation*

Let us now consider a living sample whose speckle is fully decorrelated from one frame to the next. The holograms, in planes C and A, are thus $H_{C,\text{decorr}}$ and $H_{A,\text{decorr}}$. The recorded data are analyzed by two frames detection at the tagged photon frequency, without phase shift. Indeed, the phase shift is irrelevant, because the phase is lost, from one frame to the next. We have:

$$\omega_{LO} = \omega_{LO,\text{decorr}} = \omega_L + \omega_{US} \tag{15}$$

yielding $c = 1$ in Eq. 7. The hologram $H_{C,\mathrm{decorr}}$ is calculated by:

$$H_{C,\mathrm{decorr}}(x,y) = I_0(x,y) - I_1(x,y) \tag{16}$$

The reconstructed hologram $H_{A,\mathrm{decorr}}$ is calculated from $H_{C,\mathrm{decorr}}$ by Fourier transform:

$$\begin{aligned} H_{A,\mathrm{decorr}}(X,Y) &= \tilde{H}_{C,\mathrm{decorr}}(k_x,k_y) \\ &= \mathrm{FFT}(\ H_{C,\mathrm{decorr}}(x,y)) \end{aligned} \tag{17}$$

Because of Eq.16, the hologram $H_{C,\mathrm{decorr}}$ is real (phase is zero or π). The reconstructed hologram $H_{A,\mathrm{decorr}}(X,Y)$, obtained by Eq.17, is thus symmetric with respect to $(X,Y) = (0,0)$.

4. Example of hologram calculated without decorrelation and without shot noise

Here again, let us let us neglect the shot noise and assume $I'_m = I_m$.

With this hypothesis, the terms $|E_{LO}|^2$ and $|E_{C,T}|^2$ of Eq.7 do not contribute to $H_{C,\mathrm{decorr}}$, because $|E_{LO}|^2$ do not vary with time, and because $|E_{C,T}|^2$ can be neglected. We have:

$$\begin{aligned} H_{C,\mathrm{decorr}}(x,y) \simeq \sum_{m=0}^{1} (-1)^m \left(E^*_{LO}E_{C,T}(x,y,t_m) + \text{ c.c.}\right) \\ + \sum_{m=0}^{1} (-1)^m \left|E_{C,U}(x,y,t_m)\right|^2 \end{aligned} \tag{18}$$

Here, $(c^m E^*_{LO}E_{C,T}(x,y,t_m) + \text{ c.c.})$ is a tagged photon term, which can be used to extract the tagged photon signal. On the other hand, $|E_{C,U}|^2$ is a zero order terms, related to the untagged photons. This term must be filtered off.

To illustrat how the tagged and untagged photons can be separated, we have calculated the holograms $H_{C,\mathrm{decorr}}$ and $H_{A,\mathrm{decorr}}$ with tagged or untagged photons alone.

1. With tagged photons alone, $(c^m E^*_{LO}E_{C,T}(x,y,t_m) + \text{ c.c.})$ contributes alone in Eq. 18. Because the aperture A is off axis, I_0, I_1 and thus $H_{C,\mathrm{decorr}}$, which is real, varies very fast with x: see Fig. 3 (a). It results that the reconstructed hologram $H_{A,\mathrm{decorr}}$ calculated by FFT (see Eq. 17) is zero in the center of the calculation grid, and exhibits both the $+1$ (left bright rectangle) and -1 (right rectangle) grating order images of the aperture: see Fig.3 (b).

2. With untagged photons alone, the term $|E_{C,U}|^2$ contributes alone. Because the aperture A is thin, I_0, I_1 (and thus $H_{C,\mathrm{decorr}}$) vary slowly with x: see Fig. 3 (c). It results that the reconstructed hologram $H_{A,\mathrm{decorr}}$ is zero except in the center of the calculation grid, where it exhibits a bright band of signal: see Fig. 3 (d). The width of this band is twice the width of the rectangles of Fig.3 (b).

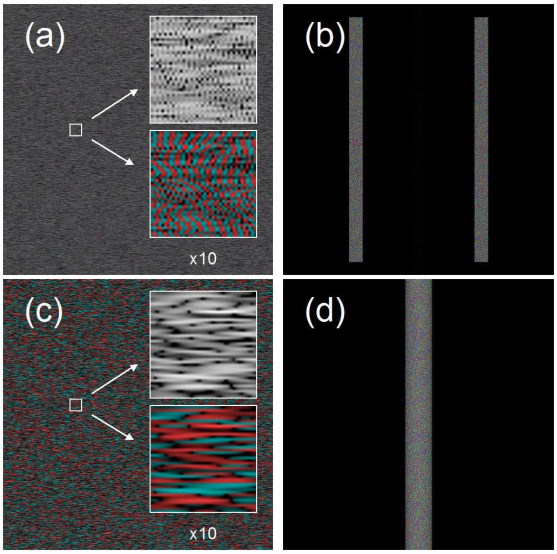


FIG. 3. (a,c) Images and $\times 10$ zoom (inserts) of the holograms $H_{C,\mathrm{decorr}}(x,y)$ calculated with decorrelation for the tagged (a) or untagged (c) photons alone. (b,d) Images of the holograms $H_{A,\mathrm{decorr}}(X,Y)$ reconstructed with tagged (b) and untagged (d) photons alone. Brightness is the amplitude in arbitrary logarithmic scale. Color is the phase. The upper zooms in (a) and (c) are displayed with amplitude alone.

The tagged and untagged contribution to the reconstructed hologram $H_{A,\mathrm{decorr}}$ are thus located in different regions of the calculation, and can be thus easily separated.

IV. THE DETECTION SENSITIVITY WITHOUT AN WITH DECORRELATION

A. The Units for the energy of the fields

To simplify the analysis, the tagged and untagged photon energies in plane A are quantified in Units of photo electron per pixel, and per T_C, where T_C is defined by the following way.

1. Without decorrelation, T_C is the recording time of the sequence of M frames. T_C is shorter than the decorrelation time.

2. With decorrelation, T_C is the exposure time of one frame. T_C is of the order of the decorrelation time, but much shorter that the camera time pitch Δt. The fields $E_{A,T}$ and $E_{A,U}$ remain thus correlated during the exposure time T_C, but are fully uncorrelated from one frame to the next.

In experiments, the local oscillator field E_{LO} can be freely adjusted. The best results are obtained by adjusting E_{LO} to be as large as possible without saturating the

camera [27–29]. We have considered a camera, whose saturation level is about 2×10^4 photo electrons, and a local oscillator power that corresponds to half saturation, i.e. $|E_{LO}| = 10^4$ photo electrons per pixel of plane C, and per frame.

In typical heterodyne UOT experiments, the tagged photon field $E_{A,T}$ is very low. It corresponds to about one photon electron per pixel or less. On the other hand, the untagged photon field $E_{A,U}$ is much larger than $E_{A,T}$, with typically $|E_{A,U}|^2/|E_{A,T}|^2 \sim 10^3$. Since the tagged photon signal is very low, it is essential to account for shot noise.

B. The reconstructed hologram H_A

To simulate the UOT experiment, we first calculated the tagged and untagged speckle fields $E_{A,T}(X, Y, t_m)$ and $E_{A,U}(X, Y, t_m)$ in plane A by Monte Carlo. We considered here a 1024×1024 calculation grid and an aperture, whose upper left and bottom right corner coordinates are $(X, Y) = (125, 0)$ and $(300, 1023)$. These parameters correspond to $x_i = -212$, $x_o = -387$, and $w = 1024$ in ΔX Units. We made the following assumption for the statistical averages $\langle|E_{A,U}|^2\rangle$, and $\langle|E_{A,T}|^2\rangle$ of the field energies $|E_{A,U}(X, Y, t_m)|^2$ and $|E_{A,T}(X, Y, t_m)|^2$ in plane A.

1. Without decorrelation, $M = 12$ (T_C is the recording time of 12 frames), $\langle|E_{A,U}|^2\rangle = 10^4$ and $\langle|E_{A,T}|^2\rangle = 1$ photo electrons per pixel and per T_C.

2. With decorrelation, $\langle|E_{A,U}|^2\rangle = 250$ and $\langle|E_{A,T}|^2\rangle = 1$ photo electrons per pixel and per T_C.

With these initial conditions, we have calculated the reconstructed hologram i.e. $H_A = H_{A,\text{corr}}$ or $H_{A,\text{decorr}}$, and displayed them in Fig. 4 (a,b).

1. Without decorrelation (Fig. 4 (a)), the tagged photon signal corresponds to the +1 image of the aperture, i.e. to the left hand side bright rectangular zone. The blurred bright zone, in the center of Fig. 4 (a), corresponds to a parasitic detection of the untagged photon signal, which does not cancel completely here because of shot noise. Finally, the shot noise yields a flat noise background in all points of the images.

2. With decorrelation (Fig. 4 (b)), the tagged photon signal corresponds to the ±1 images of the aperture, i.e. to the bright rectangular zones located in the left and right hand side of Fig. 4 (b). The blurred bright zone, in the center of Fig. 4 (b) corresponds to the untagged photon signal, which is much larger with decorrelation than without. In order to get the roughly the same brightness for the untagged photon signal, the calculation has been done with a much lower untagged energy with decorrelation (250 photo electrons) than without (10^4). Here again, the shot noise yields a flat noise background.

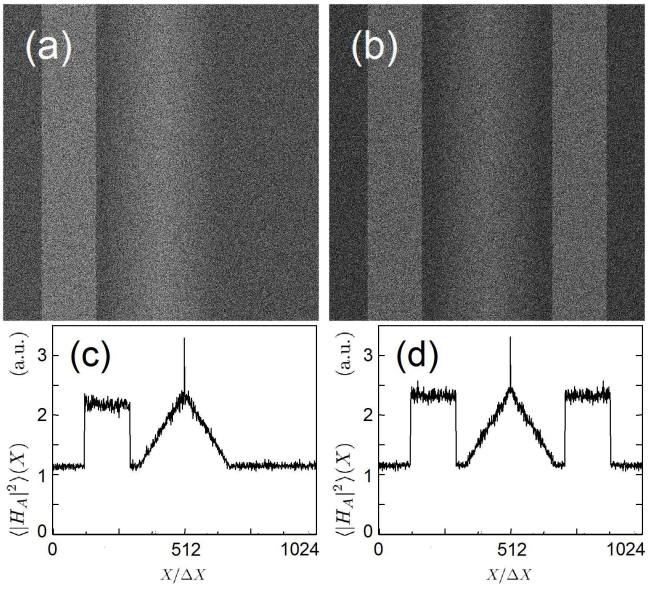


FIG. 4. Holograms $H_A(X, Y)$ (a,b) and curves $\langle|H_A|^2(X)\rangle$ (c,d) obtained by calculation with $x_i = -212$, $x_o = -387$ and $w = 1024$ in ΔX Units. The images (a,b) are displayed in an arbitrary logarithmic scale for $|H_A(X, Y)|^2$, the curves (c,d) in arbitrary linear scale.

C. The profile of H_A

To analyse more quantitatively the reconstructed hologram H_A, we have averaged $|H_A(X, Y)|^2$ over Y to get $\langle|H_A|^2\rangle(X)$ [26, 38]:

$$\langle|H_A|^2\rangle(X) = \frac{1}{N}\sum_Y |H_A(X, Y)|^2 \qquad (19)$$

where $H_A = H_{A,\text{corr}}$ without decorrelation and $H_A = H_{A,\text{decorr}}$ with.

Figure 4 (c,d) shows the curves $\langle|H_A(X)|^2\rangle$ obtained without (c) and with (d) decorrelation. The rectangular walls located on the left hand side of Fig. 4 (c) and in the left and right side of Fig. 4 (d) correspond to the tagged photon. On the other hand, the triangular walls located on the center of Fig. 4 (c) and (d) correspond to the untagged photons. The width of the triangular walls is twice the width of the rectangular walls $|x_i - x_o|$, which is equal to the width of the aperture in ΔX Units. Out of the rectangular and triangular walls, the curves exhibit a flat background noise floor that corresponds to shot noise.

Here, by a proper choice of the aperture width and aperture off axis position ($x_i = -212$, $x_o = -387$ and

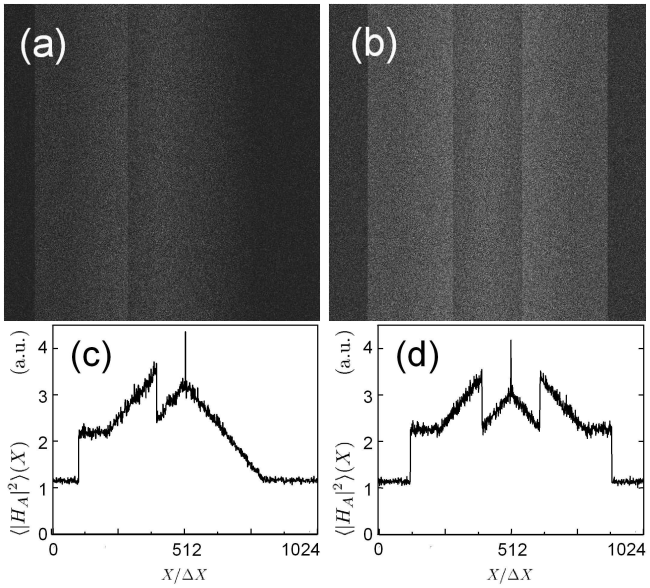


FIG. 5. Holograms $H_A(X,Y)$ (a,b) and curves $\langle|H_A|^2(X)\rangle$ (c,d) obtained by calculation with $x_i = -112$, $x_o = -387$ and $w = 1024$ in ΔX Units. The images (a,b) are displayed in an arbitrary logarithmic scale for $|H_A(X,Y)|^2$, the curves (c,d) in arbitrary linear scale.

$w = 1024$), that obedience to the conditions $|x_i| > |x_i - x_o|$ and $|x_o| < w/2$, the rectangular and triangular walls are well separated, making possible to filter off the unwanted untagged photons. Here the condition $|x_i| > |x_i - x_o|$ is needed to separate the tagged and untagged photon signals. If this condition is not fulfilled, the two signals are mixed together as shown by Fig.5, which is obtained in the same condition that Fig.4 but with $x_i = -112$, $x_o = -387$ and $w = 1024$, i.e. with $|x_i| < |x_i - x_o|$. On the other hand, the condition $|x_o| < w/2$ is needed to image the aperture properly i.e. without holographic reconstruction aliases.

By obeying to conditions $|x_i| > |x_i - x_o|$ and $|x_o| < w/2$, is also possible to select zones (like pixels 0 to 124 and 898 to 1023) without signal, where the measured signal corresponds to shot noise. Since the height of the tagged photon rectangular walls is equal to the noise floor, the shot noise equivalent signal is equal to one tagged photo electron per pixel (i.e. per etendue λ^2) and per T_C, where T_C is either the recording time of the sequence (without decorrelation), or the exposure time of one frame (with decorrelation).

D. The detection sensitivity limits

To evaluate the tagged photon detection sensitivity limits, we have calculated, without and with decorrelation, the $\langle|H_A|^2\rangle(X)$ curves by varying the tagged photon energy.

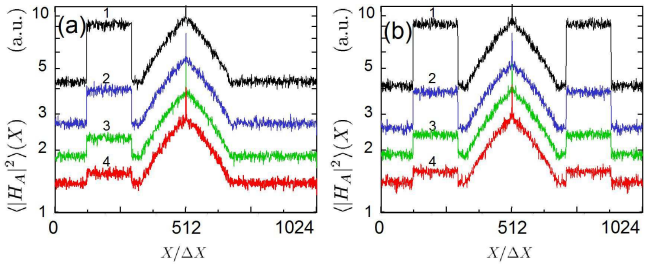


FIG. 6. Curves $\langle|H_A|^2\rangle(X)$ obtained without (a) and with decorrelation (b). Calculation is made with $\alpha = 1$ (1), 0.5 (2), 0.25 (3) and 0.125 (4), where α is the number of tagged photons per pixel and per T_C. Plots are made in arbitrary logarithmic scale.

1. Without decorrelation, the calculation is made with $M = 12$ frames, $|E_{LO}|^2 = 10^4$, $\langle|E_{A,U}|^2\rangle = 10^4$, and $\langle|E_{A,T}|^2\rangle = \alpha$ with $\alpha = 1$, 0.5, 0.25 and 0.125 for curves 1 to 4 (in photo electron per pixel of plane A, et per T_C Units).

2. With decorrelation, the calculation is made $|E_{LO}|^2 = 10^4$, $\langle|E_{A,U}|^2\rangle = 250$ and $\langle|E_{A,T}|^2\rangle = \alpha$.

The curves $\langle|H_A|^2\rangle(X)$ are drawn in Fig.6. To better visualize them, the curves were plotted in log scale, and the curves were arbitrarily shifted up or down to better separate them from each other. Figure 6 shows that we get roughly the same sensitivity for the detection of the tagged photon with and without decorrelation.

By averaging over the about 10^5 pixels of the rectangular aperture, the sensitivity limit is improved down to about $\alpha \sim 1/\sqrt{10^5} \sim 1/300$ photo electron per pixel and per T_C. This result agrees with what observed experimentally for the detection of the untagged photons [14].

V. VALIDATION OF THE THEORY WITH EXPERIMENT [26]

We have validated our theory by comparing the theoretical simulation with the experiment of ref. [26]. Since the experiment is made with low decorrelation, we have calculated $H_A = H_{A,\mathrm{corr}}$. The calculation is made with $M = 12$ frames, $|E_{LO}|^2 = 10^4$ photo electron per frames, and $\langle|E_{A,U}|^2\rangle = 3.6 \times 10^4$ and $\langle|E_{A,T}|^2\rangle = 16$ photo electron per T_C (12 frames). The size of the calculation grid is 1024×1024. The coordinates of the upper left and bottom right aperture corners are $(125, 50)$ and $(300, 974)$.

Figure 7 shows the arbitrary logarithmic scale intensity image $|H_A(X,Y)|^2$ obtained by calculation (a), and in experiment (b) [26], and the corresponding $\langle|H_A|^2\rangle(X)$ curves (c) and (d). Like in ref.[26], the curves were normalized with respect to the noise floor that corresponds to shot noise. The maximum of tagged photon signal $\langle|H_A|^2\rangle(X)$ is about 15. This figure corresponds to the

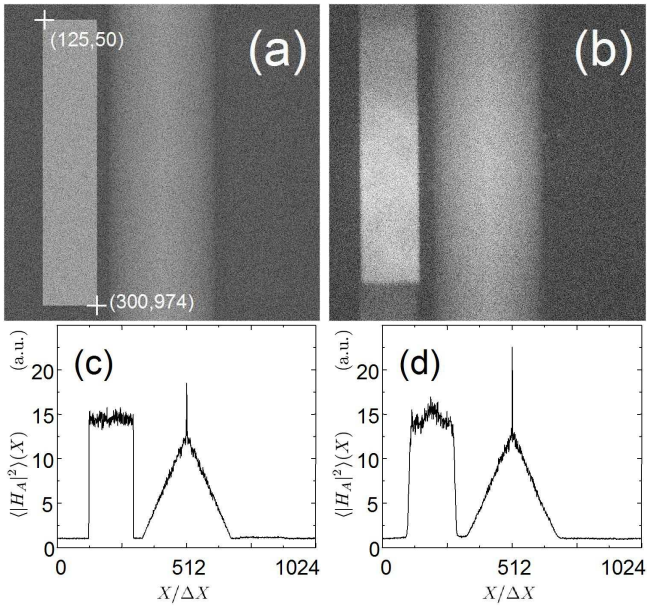


FIG. 7. Tagged intensity images $|H_A(X,Y)|^2$ (a,b) and curves $\langle|H_A(X)|^2\rangle$ (c,d) obtained by calculation (a,c) and from ref.[26] experiment (b,d). The images $|H_A(X,Y)|^2$ (a,b) are displayed in an arbitrary logarithmic scale. The curves $\langle|H_A(X)|^2\rangle$ (c,d) are normalized with respect to the ground floor.

tagged photon energy for the whose sequence of $M = 12$ frames: $\langle|E_{A,T}|^2\rangle = 16$.

The good agreement of our calculation with the experiment validates our theoretical model.

VI. CONCLUSION

In this paper, we have proposed a theoretical model to describe the detection of the tagged photons in heterodyne holography UOT. This model, which agrees with the results of [26], has been used to calculate how untagged photons, speckle noise, shot noise, decorrelation and etendue, affect the UOT signal.

By a proper choice of the aperture size, heterodyne holography UOT is able to filter off the unwanted untagged photons, and to reach a sensitivity limited by shot noise. This sensitivity corresponds to a noise equivalent signal equal to one tagged photo electron per pixel (i.e. per etendue λ^2) and per T_C, where T_C is either the recording time of the sequence (without decorrelation) , or the exposure time of one frame (with decorrelation).

We hope this work will stimulate further UOT development.

This work has been carried out thanks to the support of the LabEx NUMEV project (n° ANR-10-LABX-20) funded by the "Investissements d'Avenir" French Government program, managed by the French National Research Agency (ANR)

[1] Lihong Wang and Xuemei Zhao. Ultrasound-modulated optical tomography of absorbing objects buried in dense tissue-simulating turbid media. *Appl. Opt.*, 36(28):7277–7282, 1997.

[2] Daniel S Elson, Rui Li, Christopher Dunsby, Robert Eckersley, and Meng-Xing Tang. Ultrasound-mediated optical tomography: a review of current methods. *Interface Focus*, 1(4):632–648, 2011.

[3] Steffen G Resink, Albert C Boccara, and Wiendelt Steenbergen. State-of-the art of acousto-optic sensing and imaging of turbid media. *J. Biomed. Opt.*, 17(4):0409011–04090110, 2012.

[4] W Leutz and Georg Maret. Ultrasonic modulation of multiply scattered light. *Physica B: Condensed Matter*, 204(1):14–19, 1995.

[5] Lihong V Wang. Mechanisms of ultrasonic modulation of multiply scattered coherent light: an analytic model. *Phys. Rev. Lett.*, 87(4):043903, 2001.

[6] Lihong Wang, Steven L Jacques, and Xuemei Zhao. Continuous-wave ultrasonic modulation of scattered laser light to image objects in turbid media. *Opt. Lett.*, 20(6):629–631, 1995.

[7] M Kempe, M Larionov, D Zaslavsky, and AZ Genack. Acousto-optic tomography with multiply scattered light. *J. Opt. Soc. Am. A*, 14(5):1151–1158, 1997.

[8] Sava Sakadžić and Lihong V Wang. High-resolution ultrasound-modulated optical tomography in biological tissues. *Opt. Lett.*, 29(23):2770–2772, 2004.

[9] Sri-Rajasekhar Kothapalli and Lihong V Wang. Ultrasound-modulated optical microscopy. *J. Biomed. Opt.*, 13(5):054046–054046, 2008.

[10] Guy Rousseau, Alain Blouin, and Jean-Pierre Monchalin. Ultrasound-modulated optical imaging using a high-power pulsed laser and a double-pass confocal fabry–perot interferometer. *Opt. Lett.*, 34(21):3445–3447, 2009.

[11] Youzhi Li, Philip Hemmer, Chulhong Kim, Huiliang Zhang, and Lihong V Wang. Detection of ultrasound-modulated diffuse photons using spectral-hole burning. *Opt. Express*, 16(19):14862–14874, 2008.

[12] Youzhi Li, Huiliang Zhang, Chulhong Kim, Kelvin H Wagner, Philip Hemmer, and Lihong V Wang. Pulsed ultrasound-modulated optical tomography using spectral-hole burning as a narrowband spectral filter. *Appl. Phys. Lett.*, 93(1):011111, 2008.

[13] Huiliang Zhang, Mahmood Sabooni, Lars Rippe, Chulhong Kim, Stefan Kröll, Lihong V Wang, and Philip R Hemmer. Slow light for deep tissue imaging with ultrasound modulation. *Appl. Phys. Lett.*, 100(13):131102, 2012.

[14] M Gross, P Goy, BC Forget, M Atlan, F Ramaz, AC Boccara, and AK Dunn. Heterodyne detection of multiply scattered monochromatic light with a multipixel detector. *Opt. Lett.*, 30(11):1357–1359, 2005.

[15] Todd W Murray, Lei Sui, Gopi Maguluri, Ronald A Roy, Alex Nieva, Florian Blonigen, and Charles A Di-

Marzio. Detection of ultrasound-modulated photons in diffuse media using the photorefractive effect. *Opt. Lett.*, 29(21):2509–2511, 2004.

[16] François Ramaz, B Forget, Michael Atlan, Albert-Claude Boccara, Michel Gross, Philippe Delaye, and Gérald Roosen. Photorefractive detection of tagged photons in ultrasound modulated optical tomography of thick biological tissues. *Opt. Express*, 12(22):5469–5474, 2004.

[17] Michel Gross, François Ramaz, B Forget, Michael Atlan, A Boccara, Philippe Delaye, and Gérald Roosen. Theoretical description of the photorefractive detection of the ultrasound modulated photons in scattering media. *Opt. Express*, 13(18):7097–7112, 2005.

[18] Puxiang Lai, Xiao Xu, and Lihong V Wang. Ultrasound-modulated optical tomography at new depth. *Journal of biomedical optics*, 17(6):0660061–0660066, 2012.

[19] Salma Farahi, Germano Montemezzani, Alexander A Grabar, Jean-Pierre Huignard, and François Ramaz. Photorefractive acousto-optic imaging in thick scattering media at 790 nm with a sn 2 p 2 s 6: Te crystal. *Opt. Lett.*, 35(11):1798–1800, 2010.

[20] B Jayet, JP Huignard, and F Ramaz. Fast wavefront adaptive holography in nd: Yvo 4 for ultrasound optical tomography imaging. *Opt. Express*, 22(17):20622–20633, 2014.

[21] S Leveque, AC Boccara, M Lebec, and H Saint-Jalmes. Ultrasonic tagging of photon paths in scattering media:? parallel speckle modulation processing. *Opt. Lett.*, 24(3):181–183, 1999.

[22] Gang Yao, Shuliang Jiao, and Lihong V Wang. Frequency-swept ultrasound-modulated optical tomography in biological tissue by use of parallel detection. *Opt. Lett.*, 25(10):734–736, 2000.

[23] Jun Li and Lihong V Wang. Methods for parallel-detection-based ultrasound-modulated optical tomography. *Appl. Opt.*, 41(10):2079–2084, 2002.

[24] Jun Li, Geng Ku, and Lihong V Wang. Ultrasound-modulated optical tomography of biological tissue by use of contrast of laser speckles. *Appl. Opt.*, 41(28):6030–6035, 2002.

[25] Frédérique Le Clerc, Laurent Collot, and Michel Gross. Numerical heterodyne holography with two-dimensional photodetector arrays. *Opt. Lett.*, 25(10):716–718, 2000.

[26] Michel Gross, Philippe Goy, and Mohamed Al-Koussa. Shot-noise detection of ultrasound-tagged photons in ultrasound-modulated optical imaging. *Opt. Lett.*, 28(24):2482–2484, 2003.

[27] Michel Gross and Michael Atlan. Digital holography with ultimate sensitivity. *Opt. Lett.*, 32(8):909–911, 2007.

[28] Frédéric Verpillat, Fadwa Joud, Michael Atlan, and Michel Gross. Digital holography at shot noise level. *J. Displ. Techn.*, 6(10):455–464, 2010.

[29] Max Lesaffre, Nicolas Verrier, and Michel Gross. Noise and signal scaling factors in digital holography in weak illumination: relationship with shot noise. *Appl. Opt.*, 52(1):A81–A91, 2013.

[30] Yan Liu, Yuecheng Shen, Cheng Ma, Junhui Shi, and Lihong V Wang. Lock-in camera based heterodyne holography for ultrasound-modulated optical tomography inside dynamic scattering media. *Appl. Phys. Lett.*, 108(23):231106, 2016.

[31] Kinia Barjean, Kevin Contreras, Jean-Baptiste Laudereau, Éric Tinet, Dominique Ettori, François Ramaz, and Jean-Michel Tualle. Fourier transform acousto-optic imaging with a custom-designed cmos smart-pixels array. *Opt. Lett.*, 40(5):705–708, 2015.

[32] Michael Atlan, Michel Gross, Benoit C Forget, Tania Vitalis, Armelle Rancillac, and Andrew K Dunn. Frequency-domain wide-field laser doppler in vivo imaging. *Opt. Lett.*, 31(18):2762–2764, 2006.

[33] Michael Atlan and Michel Gross. Laser doppler imaging, revisited. *Rev. Scientific Instr.*, 77(11):116103, 2006.

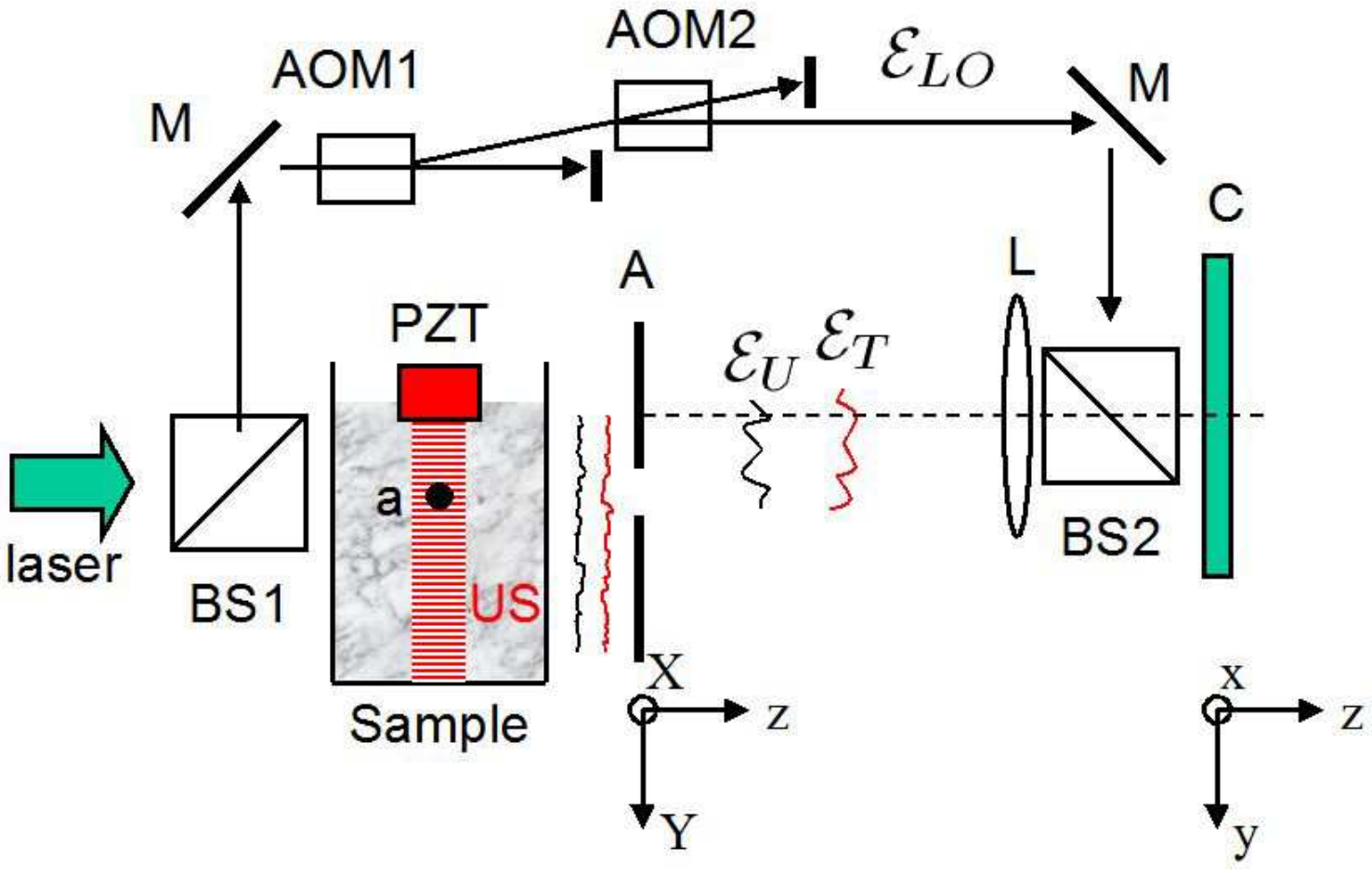
[34] Max Lesaffre, Michael Atlan, and Michel Gross. Effect of the photon's brownian doppler shift on the weak-localization coherent-backscattering cone. *Phys. Rev. Lett.* , 97(3):033901, 2006.

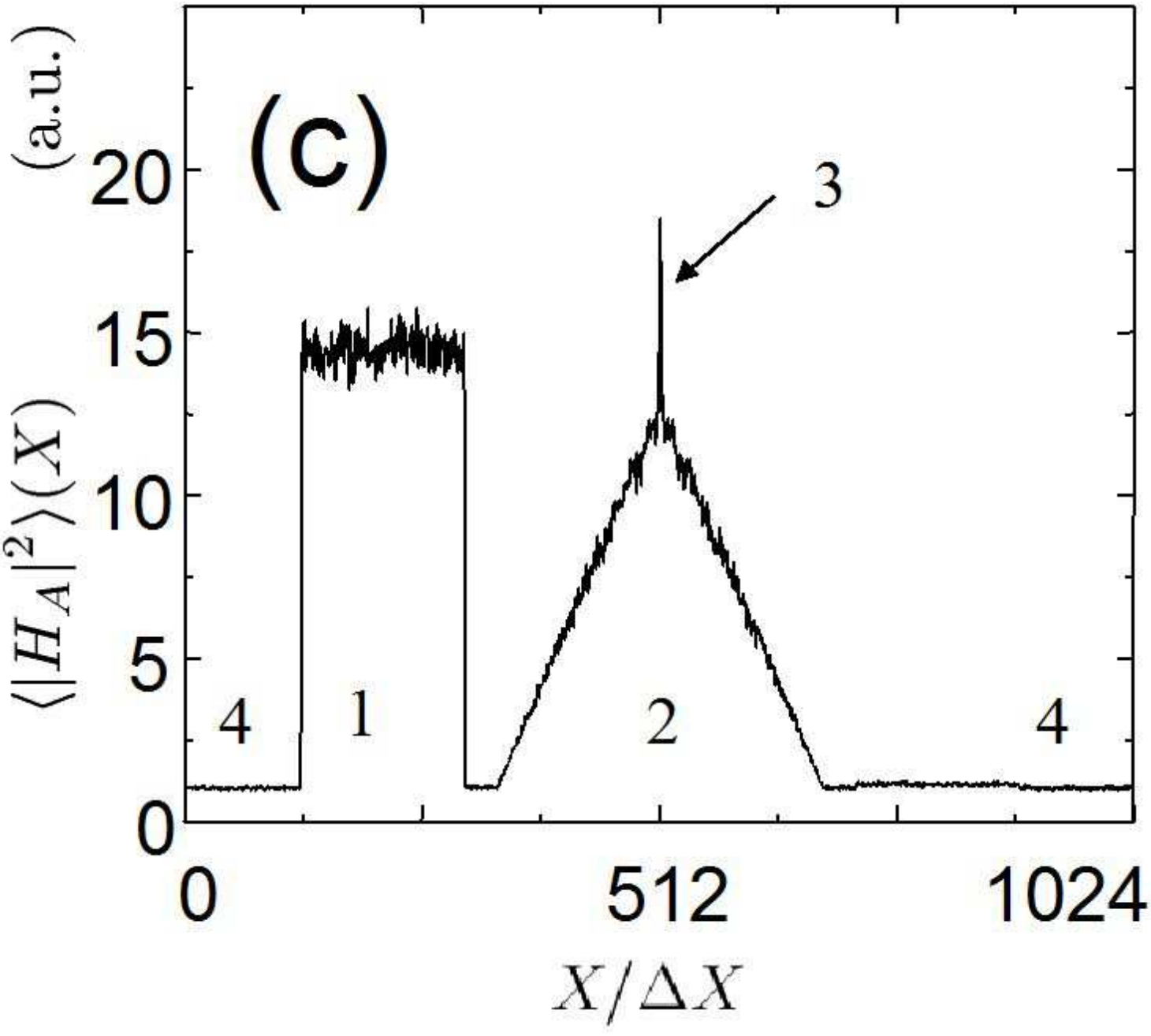
[35] Michael Atlan, Benoit C Forget, Albert C Boccara, Tania Vitalis, Armelle Rancillac, Andrew K Dunn, and Michel Gross. Cortical blood flow assessment with frequency-domain laser doppler microscopy. *J. Biomed. Opt.*, 12(2):024019–024019, 2007.

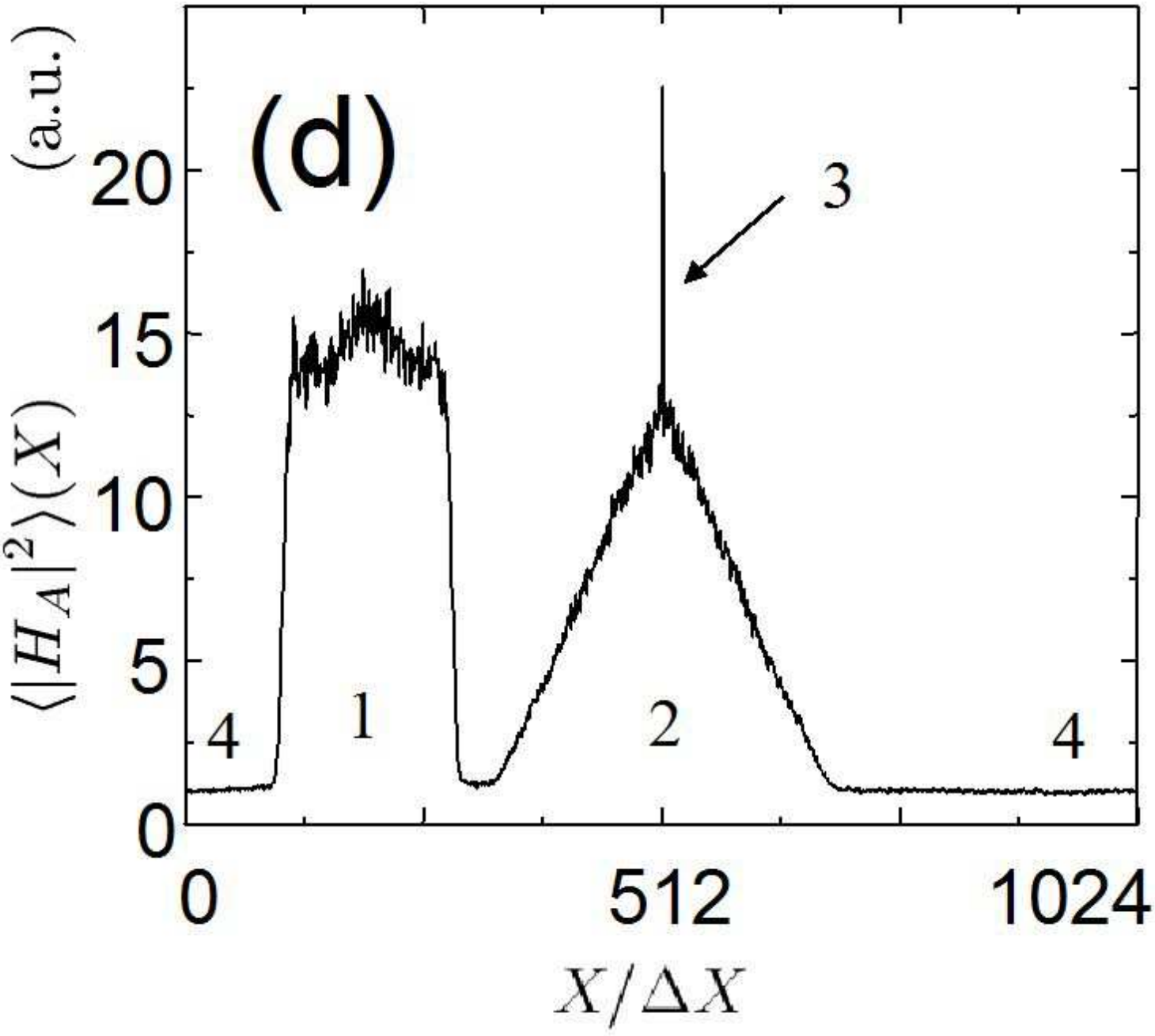
[36] Michael Atlan and Michel Gross. Spatiotemporal heterodyne detection. *J. Opt. Soc. Am. A*, 24(9):2701–2709, 2007.

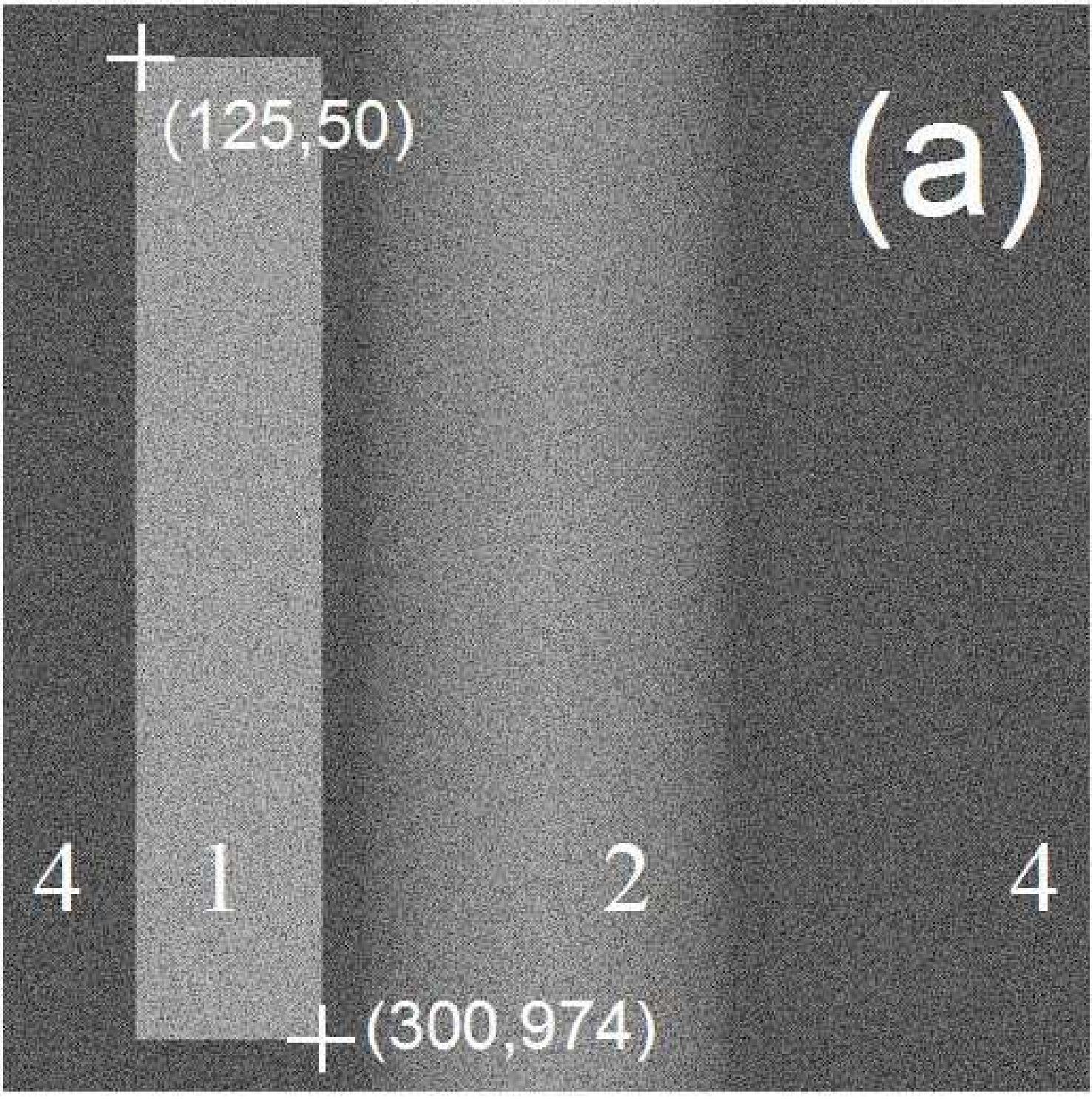
[37] Michael Atlan, Michel Gross, Tania Vitalis, Armelle Rancillac, Jean Rossier, and AC Boccara. High-speed wave-mixing laser doppler imaging in vivo. *Opt. Lett.*, 33(8):842–844, 2008.

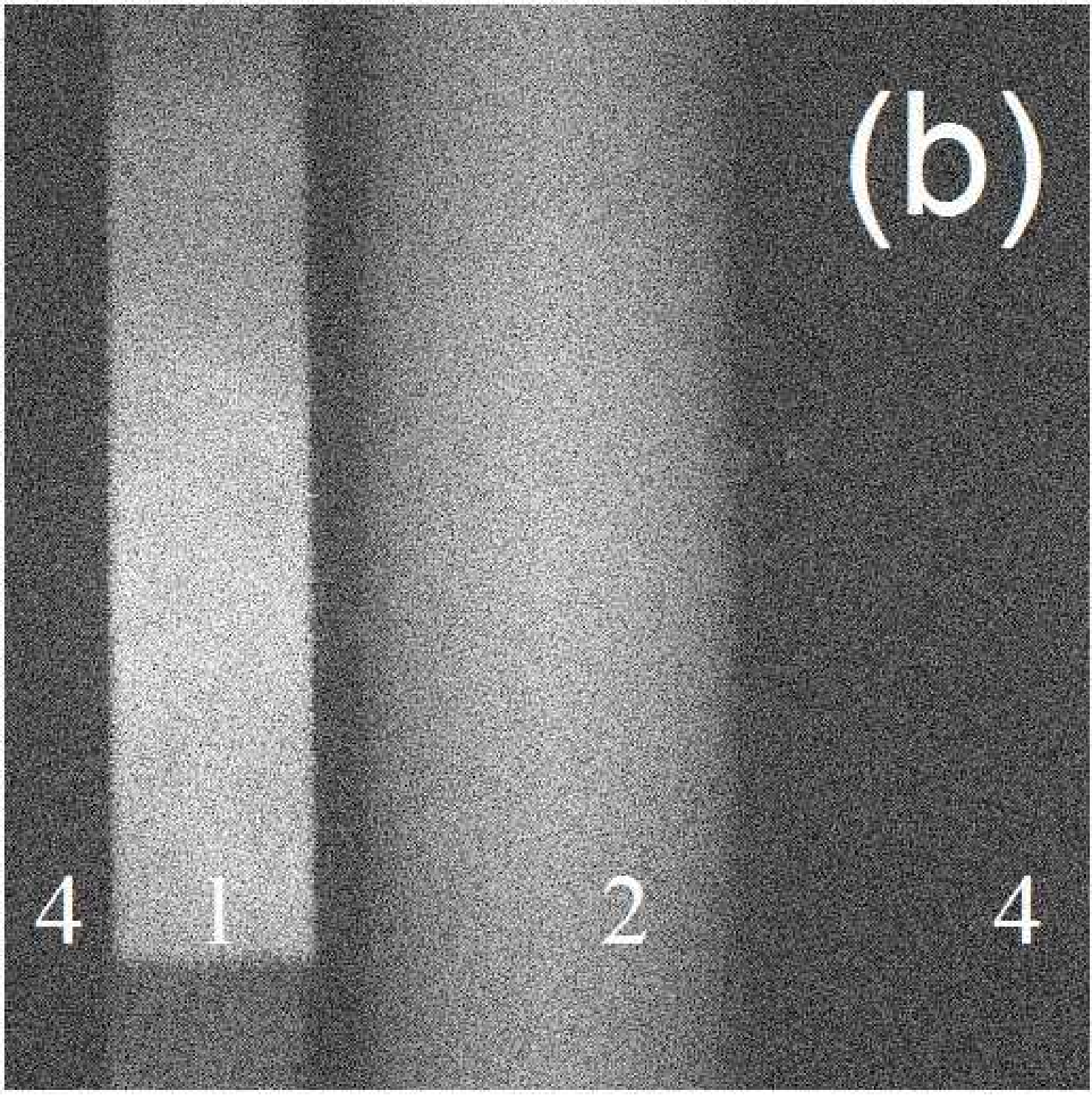
[38] Haowen Ruan, Melissa L Mather, and Stephen P Morgan. Pulsed ultrasound modulated optical tomography with harmonic lock-in holography detection. *J. Optc. Soc. Am. A* , 30(7):1409–1416, 2013.

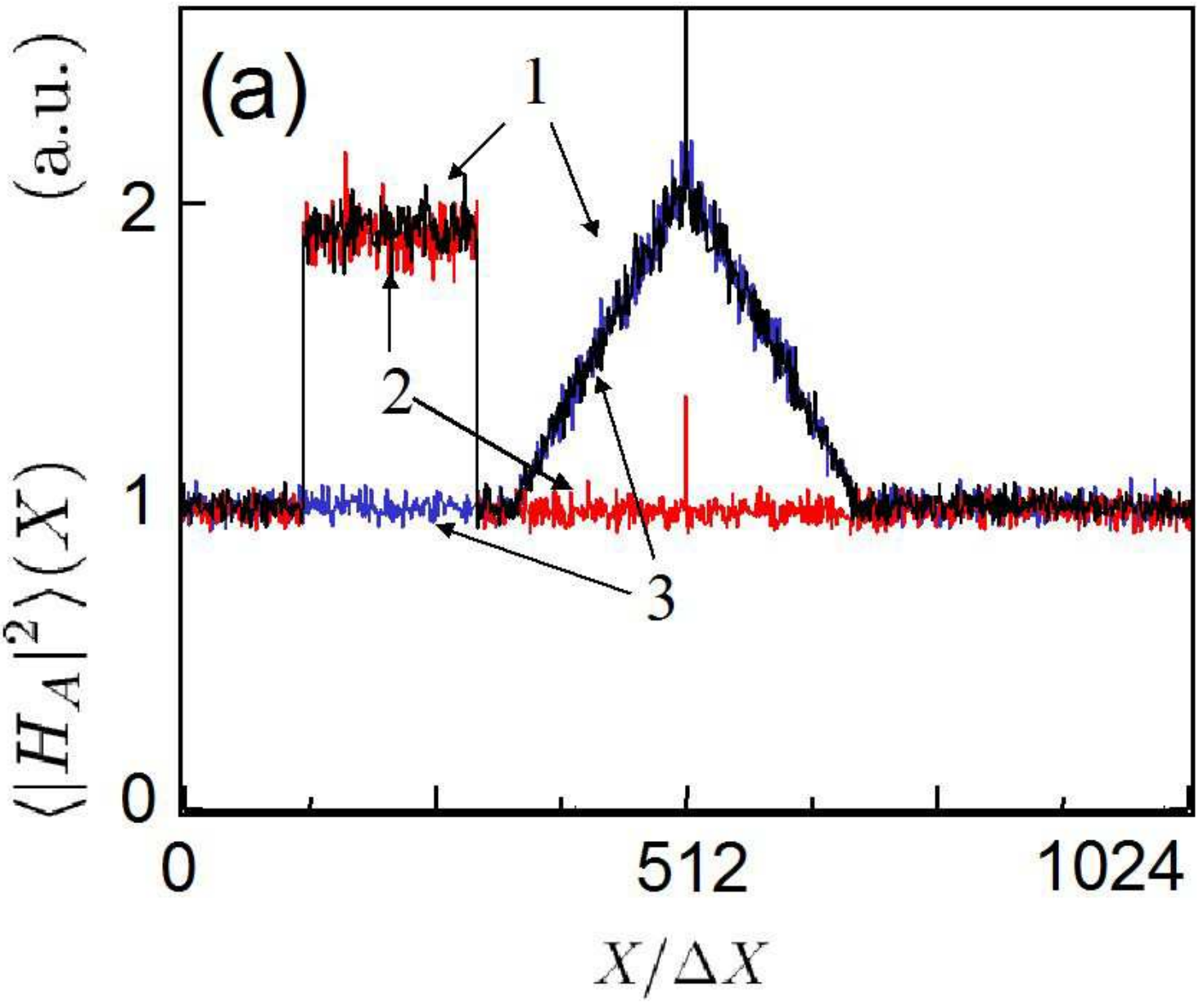

AOM2
AOM1
$\mathcal{E}_{LO}$
M
M
C
L
A
PZT
$\mathcal{E}_U$ $\mathcal{E}_T$
a
laser
BS1
US
BS2
Sample
X
z
Y
x
z
y

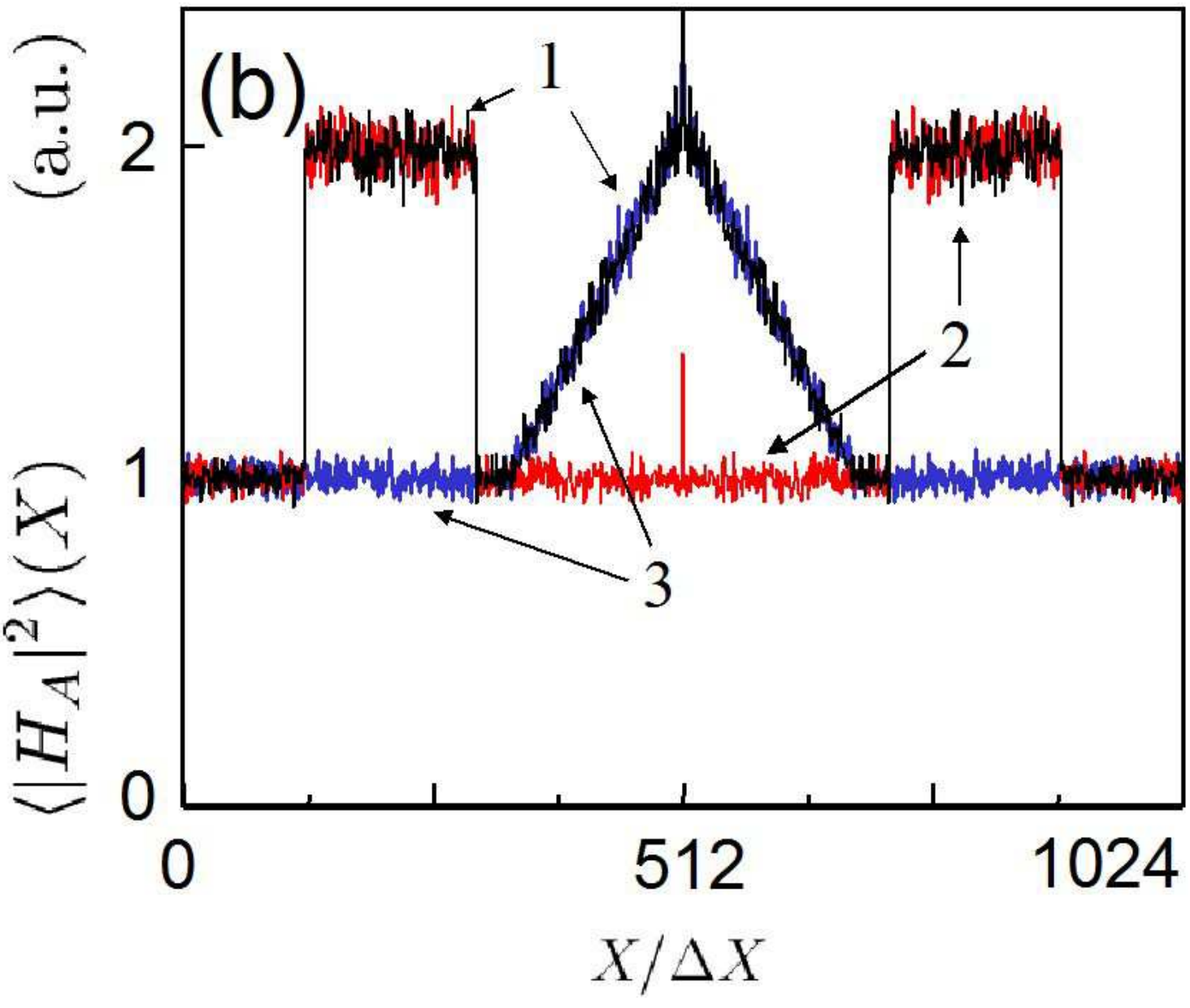

(c)
(a.u.)
$\langle |H_A|^2 \rangle (X)$
20
15
10
5
0
0
512
1024
$X/\Delta X$
1
2
3
4
4

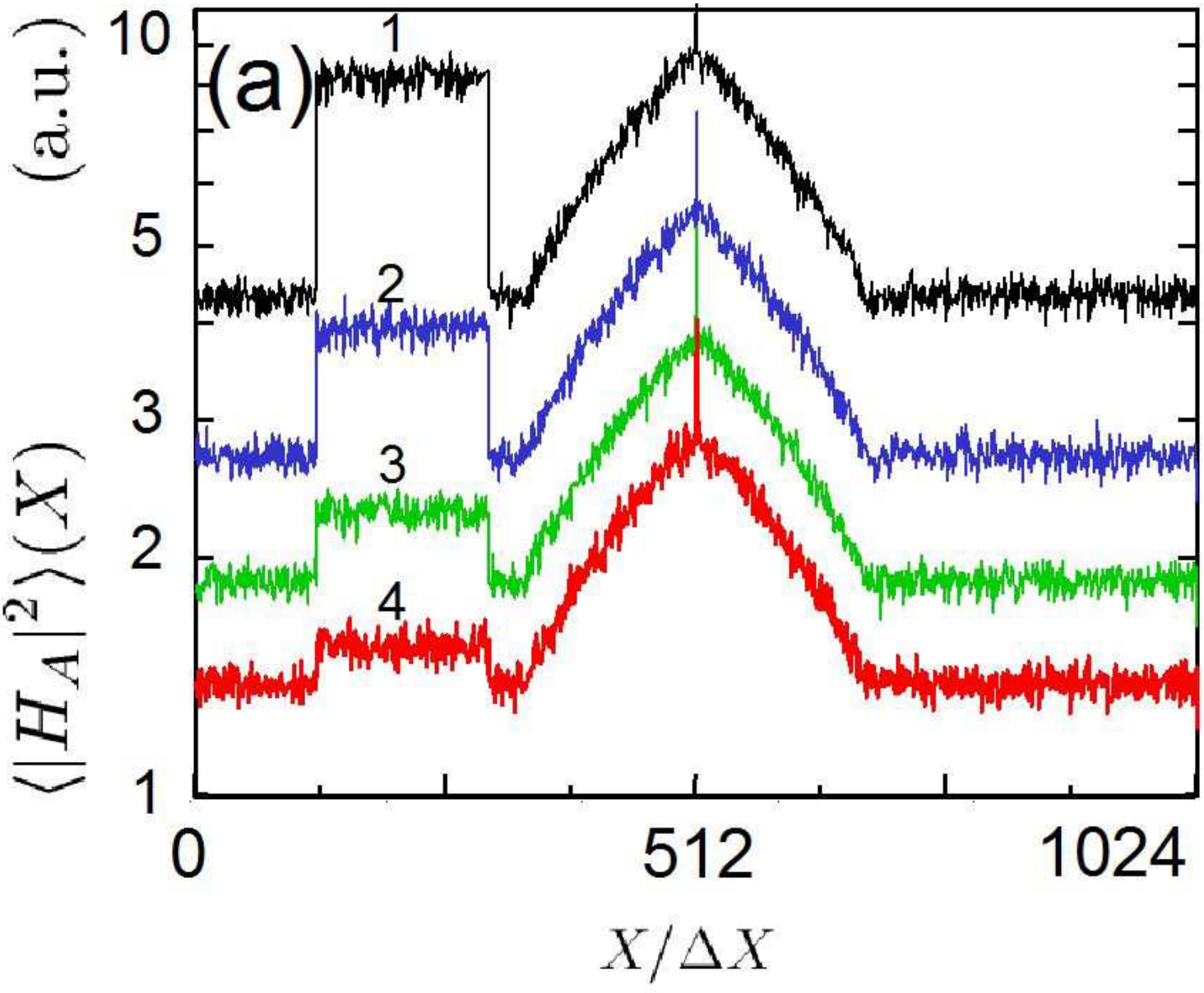

(d)
(a.u.)
$\langle |H_A|^2 \rangle (X)$
20
15
10
5
0
0
512
1024
$X/\Delta X$
1
2
3
4
4

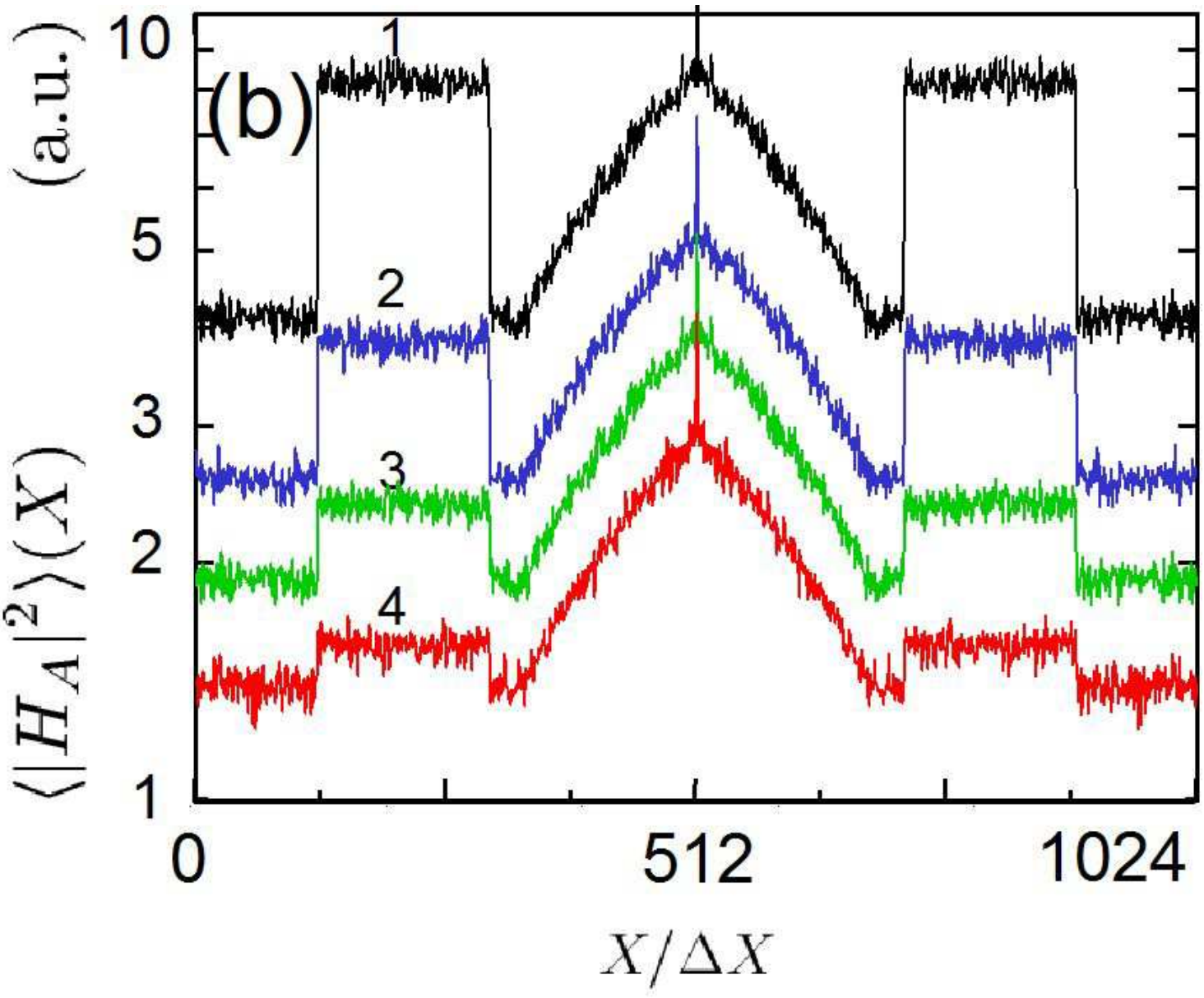

(125,50)
(a)
4
1
2
4
(300,974)


(b)
4
1
2
4


(a)
1
2
3
2
1
0
0
512
1024
(a.u.)
$\langle |H_A|^2 \rangle (X)$
$X/\Delta X$


(b)
1
2
3
2
1
0
0
512
1024
(a.u.)
$\langle |H_A|^2 \rangle (X)$
$X/\Delta X$


(a)
1
2
3
4
10
5
3
2
1
0
512
1024
(a.u.)
$\langle |H_A|^2 \rangle (X)$
$X/\Delta X$


(b)
1
2
3
4
10
5
3
2
1
0
512
1024
(a.u.)
$\langle |H_A|^2 \rangle (X)$
$X/\Delta X$